doi: 10.25750/1995-4301-2025-3-119-133

Dye wastewater treatment using lignin from durian rind (*Durio zibethinus* Rumph. ex Murray)

© 2025. Tran Y Doan Trang[1] ORCID: 0000-0003-3945-7748, Lai Hong Dzung[2] ORCID: 0000-0002-2696-0099, Do Thi Cam Van[1] ORCID: 0000-0002-6564-3934, Ta Thi Huong[1] ORCID: 0000-0002-1627-4124, Nguyen Quang Tung[1] ORCID: 0000-0002-0962-0332, Thi-Dung Ha[1] ORCID: 0009-0004-6599-6475, Do Thi Hanh[1] ORCID: 0000-0002-1051-836X, Vu Phuong Lan[1] ORCID: 0009-0005-9451-4698,
[1]Hanoi University of Industry,
298, Cau Dien St., Hanoi, Vietnam, 11900,
[2]Kazan National Research Technological University,
68, Karl Marx St., Kazan, Russia, 420015,
e-mail: tydtrang@gmail.com, tydtrang@haui.edu.vn

The agricultural sector is generating increasing amounts of solid waste, leading to a growing trend of reusing or recycling these waste materials into valuable resources. This study evaluated the potential of lignin extracted from durian rind (DR) to remove methylene blue (MB) dye from wastewater. Lignin samples were characterized using Fourier transform infrared spectroscopy, optical microscopy, scanning electron microscopy, and thermal analysis. The impact of different factors, including pH, initial MB concentration, adsorbent dosage, and contact time, was evaluated in the batch adsorption experiments. The data showed that the maximum adsorption capacity of the lignin from DR occurred at pH of 5, with an adsorbent dosage of 10 $g \cdot L^{-1}$ and a contact time of 60 minutes. Kinetic studies showed that the adsorption process was well described by a pseudo-second-order kinetic model with a high adsorption capacity of 40.16 $mg \cdot g^{-1}$. Additionally, the adsorption isotherm results aligned well with the Langmuir equation, indicating monolayer adsorption on a homogeneous surface. The physical adsorption mechanism was proposed to involve electrostatic interactions, ϖ interactions, and hydrogen bonding between the adsorbate and the adsorbent. In conclusion, this study highlights the potential for agricultural waste, such as durian rind, to be repurposed into effective adsorbent materials for treating dye contamination in water environments.

Keywords: lignin, durian rind, methylene blue, isotherm, kinetic, adsorption.

УДК 628.34, 674.8, 627.4

Очистка сточных вод от красителей с использованием лигнина из кожуры дуриана (*Durio zibethinus* Rumph. ex Murray)

© 2025. Чан И Доан Чанг[1], к. т. н., преподаватель, Лай Хонг Зунг[2], аспирант, До Тхи Кам Ван[1], к. т. н., преподаватель, Та Тхи Хыонг[1], к. т. н., преподаватель, Нгуен Куанг Тунг[1], к. т. н., доцент, Тхи-Зунг Ха[1], к. т. н., преподаватель, До Тхи Хань[1], к. т. н., преподаватель, Ву Фыонг Лан[1], к. т. н., преподаватель,
[1]Ханойский промышленный университет,
11900, Вьетнам, г. Ханой, ул. Каудыен, д. 298,
[2]Казанский национальный исследовательский технологический университет,
420015, Россия, г. Казань, ул. Карла Маркса, д. 68,
e-mail: tydtrang@gmail.com, tydtrang@haui.edu.vn

Сельскохозяйственный сектор производит всё большее количество твёрдых отходов, в связи с этим возникает вопрос о повторном использовании или переработке этих отходов в ценные ресурсы. В данном исследовании оценивался потенциал лигнина, извлечённого из кожуры дуриана *Durio zibethinus* Rumph. ex Murray, для удаления красителя метиленового синего из сточных вод. Образцы лигнина были изучены методами инфракрасной Фурье-спектроскопии, оптической микроскопии, сканирующей электронной микроскопии и термического анализа. В экспериментах по адсорбции было оценено влияние различных факторов, включая pH, начальную концентрацию метиленового синего, дозировку адсорбента и время контакта. Результаты показали, что максимальная адсорбционная способность лигнина из дуриана наблюдалась при pH 5, дозировке адсорбента 10 г/л и времени контакта 60 минут. Кинетические исследования показали, что процесс адсорбции подчинялся кинетической модели псевдовторого

порядка с высокой адсорбционной способностью 40,16 мг/г. Результаты адсорбционной изотермы хорошо согласовывались с уравнением Лэнгмюра, указывая на мономолекулярную адсорбцию на однородной поверхности. Было предположено, что механизм физической адсорбции включает электростатические взаимодействия, π-взаимодействия и водородные связи между адсорбатом и адсорбентом. Это исследование подчёркивает потенциал сельскохозяйственных отходов, таких как кожура дуриана, для преобразования в эффективные адсорбционные материалы для очистки промышленных сточных вод от загрязнения красителями.

Ключевые слова: лигнин, кожура дуриана, метиленовый синий, изотерма, кинетика, адсорбция.

Dyes are extensively utilized across various industries, including textiles, cosmetics, printing, paints, plastics, food, pharmaceuticals, and photography [1–3]. During the dyeing process, approximately 10–15% of the dye content enters the environment following production and processing [1, 3–5]. However, dye molecules are known for their colourfastness and high resistance to degradation due to their complex chemical properties [1, 3]. Textile dye wastewater often contains high levels of colour and salinity, elevated temperatures, varying pH levels, and high levels of chemical oxygen demand. Pollution from dye-containing wastewater is a significant concern as it negatively impacts the aesthetic qualities, water clarity, and gas solubility in aquatic environments. This affects marine life and presents numerous environmental challenges [4]. Most synthetic dyes are toxic, mutagenic, carcinogenic, and posing severe health risks to humans [1]. Even concentrations of dyes lower than 1 mg/L can be visibly observed and harm human health. For example, methylene blue (MB) dye, commonly used for dyeing cotton, wood, fabrics, fibres, plastics, and other materials, is hazardous and can potentially cause increased heart rate, nausea, shock, skin discolouration, anaemia, eye irritation, paralysis, tissue necrosis, methemoglobinemia, confusion, carcinogenesis, and mutagenesis [1, 6 12]. The dyes presence in water also disrupts light penetration, reduces photosynthesis, disrupts natural food chains, and increases overall chemical oxygen demand, leading to eutrophication, chemical pollution, disturbance of aquatic life, and environmental degradation [3, 13]. Therefore, the urgent removal of dyes from wastewater is imperative.

There are numerous methods for removing dyes from wastewater, including biological processes, chemical precipitation, advanced oxidation processes, photocatalytic degradation, reverse osmosis, nanofiltration, membrane separation, electrocoagulation, and ion exchange [2, 3, 14–18]. However, these modern techniques require significant energy, chemical consumption, operational costs, large initial investments, high capital expenditure, and skilled technological expertise [4]. In contrast, adsorption methods are simple, cost-effective, highly efficient, easy to design, and environmentally friendly [3, 4, 19–22].

In recent years, a significant focus has been given to developing adsorbents from agricultural and industrial waste, which are by-products of lignocellulosic biomass sources. These materials have gained attention due to their low cost and easy availability. Various adsorbents derived from agricultural waste have been researched for their effectiveness in removing MB from wastewater. These include activated carbons from agricultural waste [4], sawdust biochars [3], adsorbents derived from carboxylate-modified agro-forestry residues [18], nanocrystalline cellulose from waste paper [17], and adsorbents derived from agricultural waste such as wheat straw [14] and sisal fibre [12]. This trend helps manage solid waste sources and leads to developing practical products for various applications.

Agricultural biomass is a valuable natural resource, but it also poses challenges regarding secondary pollution and the sheer volume of waste generated. One notable example of agricultural waste impacting the environment is durian rind. *Durian zibethinus* Rumph. ex Murray, renowned for its high nutritional value and distinctive flavour, enjoys global popularity, resulting in a considerable increase in rind waste production [23]. It is estimated that approximately 480 thousand tons of this waste are generated annually [23, 24]. Durian rind (DR), comprising cellulose, pectin, lignin, polyphenols, and flavonoids, holds promise as a renewable resource for addressing waste management issues and extracting valuable components. Lignin, constituting 10 15% of DR and currently discarded into the environment, contributes to complex wastewater challenges. Recent studies demonstrate that lignin's porous structure enables effective use in wastewater treatment through adsorption mechanisms. Moreover, lignin's aromatic ring structure and functional groups like ethers and hydroxyls enhance its ability to absorb heavy metal ions, dyes, and organic pollutants effectively [25–29]. Therefore, lignin emerges as a promising adsorbent mate-

rial, highlighting the potential loss of valuable lignin resources due to the annual disposal of significant agricultural waste.

This study uses lignin recovered from DR to adsorb MB dye in water. The properties of the recovered lignin were evaluated using infrared spectroscopy (FTIR), optical microscopy, surface morphology analysis by scanning electron microscopy (SEM), and thermal analysis (TG/DTG). Various experimental parameters such as pH, initial dye concentration, contact time, and adsorbent dosage were carefully studied. The adsorption mechanism was analyzed using kinetic models, including first-order and second-order kinetics, intraparticle diffusion, the Boyd equation, and equilibrium data fitted to Langmuir, Freundlich, Temkin, and Dubinin-Radushkevich isotherm models.

Material and methods

Durian rind was utilized for lignin extraction. The durian rinds were obtained from Hanoi, Vietnam. The raw material was then cleaned, cut into small pieces, and dried to a constant weight using a vacuum oven. After drying, the durian rinds were ground into a powder with a particle size of 250 μm and stored in low-moisture, low-light conditions at the room temperature. In this study, various chemicals were used, including sodium hydroxide (Vietnam), sulfuric acid (China), and methylene blue (purity >99%, Germany).

Extraction of lignin from DR. The lignin extraction process was performed as described by Sabe et al. [3]. Initially, DR powder was heated in a 15% (w/v) NaOH solution with a solvent ratio of 20:1 mL/g at 100 °C for 2 hours. After heating, the mixture was filtered, and the liquid portion, known as black liquor, was collected. Concentrated H_2SO_4 was added to the black liquor until the pH 1. The mixture was left to stand for 24 hours, followed by filtration and washing with distilled water until a neutral pH was achieved. The solid residue on the filter paper was dried to a constant weight to obtain lignin in the powder form.

Fourier-transform infrared spectroscopy (FTIR). The FTIR was utilized to analyze the functional groups present in lignin extracted from DR. The sample was pelletized with KBr and analyzed using a spectrometer Nicolet 5700 (Thermo Fisher Scientific, USA). Spectral analysis covered the wavelength range from 400 cm^{-1} to 4000 cm^{-1} with a resolution of 4 cm^{-1}.

The SEM surface morphology and optical microscopy images. The SEM (JSM-6500, JEOL, USA) was used to analyzed the surface morphology of lignin with an acceleration voltage of 20 kV. Furthermore, optical microscopy images of lignin were observed using a trinocular optical microscope (Leica DM750, Olympus, Japan), at magnifications ranging from ×50 to ×1000.

TG and DTG. The thermal analysis was performed using a TG/DTG instrument (STA6000, PerkinElmer, USA) with a temperature range of 30 to 600 °C, a heating rate of 3 °C/min, under a nitrogen (N_2) atmosphere. The sample mass was approximately 2.5 mg, and a dynamic atmosphere of synthetic air (50 mL/min) was maintained.

Adsorption methylene blue (MB). A stock solution of MB was prepared at an initial concentration of 2000 mg/L. Batch adsorption experiments were conducted by adding lignin powder to the MB solution at adsorbent dosages ranging from 2 to 20 g/L, MB concentrations varying between 250 mg/L and 2000 mg/L, pH levels ranging from 3.0 to 9.0, and contact times from 5 to 180 minutes at room temperature. pH adjustments were made using 1M NaOH or 1M HCl solutions. The mixtures were continuously stirred during the adsorption process and subsequently filtered using filter paper. The remaining MB concentration was determined at a wavelength of 664 nm using a spectrophotometer UV-VIS nano (Nabi, MicroDigital, Korea). The adsorption capacity (q_e, mg/g) was calculated using equation (1), and the removal efficiency (R, %) was determined using equation (2) [3, 30–31]:

$$q_e = \frac{(C_0 - C_t) \cdot V}{m} \quad (1)$$

$$R = \frac{C_0 - C_t}{C_0} \quad (2) \quad (2)$$

where q_e – the adsorption capacity, mg/g; C_0 and C_t – the initial and remaining MB concentration, respectively, mg/mL; m – adsorbent weight, g; V – MB solution volume, L.

Equilibrium models. The Langmuir adsorption isotherm, represented by equation (3), was a widely used model in adsorption studies. It was assumed that adsorption occurs on a homogeneous surface, forming a monolayer with no interaction between adsorbed molecules [32, 33].

$$\frac{C_e}{q_e} = \frac{1}{q_m \cdot K_L} + \frac{C_e}{q_m} \quad (3)$$

where C_e – the equilibrium adsorbate concentration, mg/mL; q_e – the adsorption capacity, mg/g; q_m – maximum adsorption capacity, mg/g; K_L – the Langmuir constant, L/mg;

According to the Langmuir model, the dimensionless separation factor constant R_L was calculated using equation (4):

$$R_L = \frac{1}{1+K_L \cdot C_e} \quad (4)$$

The Freundlich adsorption isotherm model characterizes multilayer adsorption, where heat and adsorption affinity are uneven across a heterogeneous surface, as represented by equation (5) [1, 34]. According to the Freundlich model, the adsorption energy at different active sites is different [3, 34, 35].

$$\ln q_e = \ln K_F + \frac{1}{n} \ln C_e \quad (5)$$

where K_F – the Freundlich constant related to adsorption capacity, mg/g; 1/n – the parameter related to adsorption intensity.

The Dubinin-Radushkevich model (D-R) was studied to provide information on whether the nature of the adsorption was physical or chemical by evaluating the adsorption energy E from equation (6) [33, 36]:

$$\ln q_e = \ln q_m - \left(\frac{RT}{E}\right)^2 \ln\left(\frac{C_s}{C_e}\right)^2 \quad (6)$$

where C_s – the initial sorbate concentration, mg/mL; T – the temperature of the system, K; R – the universal gas constant ($R = 8.314 \cdot 10^{-3}$ kJ/mol); E – the adsorption energy, kJ/mol.

The Temkin model was represented by equation (7) [3, 32, 33, 37]:

$$q_e = \frac{R \cdot T}{b_{TE}} \ln a_{TE} + \frac{R \cdot T}{b_{TE}} \ln C_e \quad (7)$$

where a_{TE} – the binding constant at equilibrium (sorption equilibrium constant) corresponding to the maximum binding energy; b_{TE} – the Temkin constant.

Kinetic models. The kinetics of MB adsorption onto lignin extracted from DR were evaluated using the pseudo-first-order, pseudo-second-order, intraparticle diffusion models, and the Boyd equation.

The pseudo-first-order model was described by equation (8) [31, 38]:

$$q_t = q_e(1 - e^{-k_1 \cdot t}), \quad (8)$$

where q_e and q_t are the adsorption capacity at equilibrium status and time t, mg/g; k_1 – the rate constant for the pseudo-first-order kinetic model, min^{-1}.

The pseudo-second-order kinetic model could be described by equation (9) [31, 39]:

$$q_t = \frac{k_2 q_e^2 t}{1+k_2 q_e t} \quad (9)$$

where k_2 – the rate constant for the pseudo-second-order kinetic model, g/g·min;

The initial adsorption rate was expressed as equation (10):

$$h = k_2 q_e^2 \quad (10)$$

where h – the initial adsorption rate, mg/g·min.

The linear of the intraparticle diffusion model was expressed by the equation (11) [3, 31, 32, 40]:

$$q_t = k_p \cdot t^{0.5} + C \quad (11)$$

where k_p – the intraparticle diffusion rate constant, mg/g·min; C – a constant related to the bounding layer thickness.

The Boyd equation was expressed by equation (12) [3, 37].

$$\ln(1-F) = -\gamma \cdot t \quad (12)$$

where F – the degree of equilibrium in the system, which is calculated by the formula $F = q_t / q_e$; γ – the unitless constant; B_t – the dimensionless Boyd parameter, which is determined from F, cm^2/s, as equations (13) and (14):

for $F \leq 0.85$:

$$B_t = \left(\sqrt{\pi} - \sqrt{\pi - \left(\frac{\pi^2 F}{3}\right)}\right)^2, \quad (13)$$

for $F > 0.85$:

$$B_t = -0.498 - \ln(1-F). \quad (14)$$

Data analysis. The experimental data was analysed using Microsoft Excel. The adsorption kinetic and isotherm models were analysed through linear regression using the least squares method in Microsoft Excel to estimate the model parameters from the linear equations directly. Each experiment was performed three times.

Results and discussion

FTIR. The chemical structure of lignin obtained from DR is depicted in the FTIR spectrum results shown in Figure 1. The peak at 3348.34 cm^{-1} is characteristic of OH stretching bonds in phenolic and aliphatic hydroxyl groups [25, 30, 41]. Absorption at 2925.07 cm^{-1} indicates symmetric and asymmetric C–H stretching of the -CH_3 group [25]. The -C=O stretching vibration of the carboxylic groups in lignin appears at 1710.38 cm^{-1}. Peaks at 1632.95 cm^{-1} are attributed to aromatic skeletal vibrations within the lignin structure [25, 42, 43]. The band at 1429.81 cm^{-1} represents -CH_2 group stretching [25, 41, 44]. The peak at 1044.01 cm^{-1} signifies aromatic C–H in-plane deformation. Peaks at 605.57 and 897.19 cm^{-1} indicate the presence of guaiacyl (G), and hydro-phenyl (H) [25, 45, 46]. The spectrum of the obtained lignin is comparable to FTIR spectra of organosolv lignin from rice straw [1], lignin recovered from the formic acid process [47], eucalyptus wood powder [48], and lignin obtained from various plants [49], as well as lignin from Moroccan thuya wood [50] and softwood kraft lignin nanoparticles [41], lignin from sugarcane bagasse [30], lignin extracted from native *Leucaena leucocephala* bark [51].

Optical microscopy image and surface morphology. The optical microscopy image of lignin at ×100 magnification clearly shows that the lignin particles obtained from DR are granular in form. These lignin particles tend to aggregate strongly. Similar aggregation of lignin particles has been reported for organosolv lignin from rice straw [25] and for ethanol-based lignin [52]. The structure of lignin contains many carbonyl, phenolic, and aliphatic hydroxyl groups, which can form hydrogen bonds with each other. This results in the occurrence of mutual solid attraction forces between the lignin particles, leading to aggregation, as shown in Figure 2.

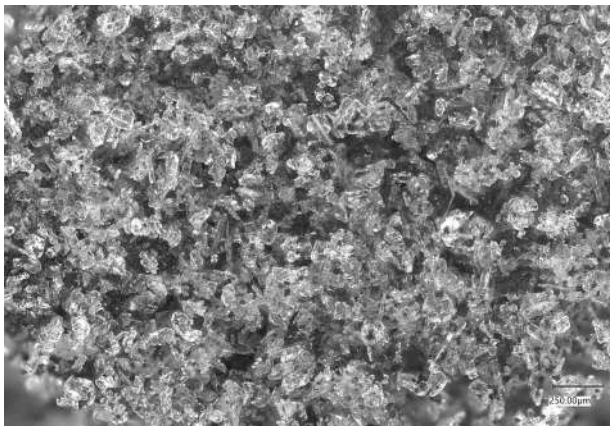

Fig. 2. Optical microscopic image of lignin from durian rind

The surface morphology SEM images of lignin isolated from DR, depicted in Figure 3, vividly illustrate the morphological characteristics of the lignin particles. The DR lignin structure consists of predominantly compact and relatively uniform interconnected particles that tend to aggregate into large conglomerates [53]. The surface of the lignin mass appears rough and uneven, marked by microscopic pores. This irregular pattern is attributed to the complex, amorphous nature of lignin polymer chains [41], which enhances the contact area between the

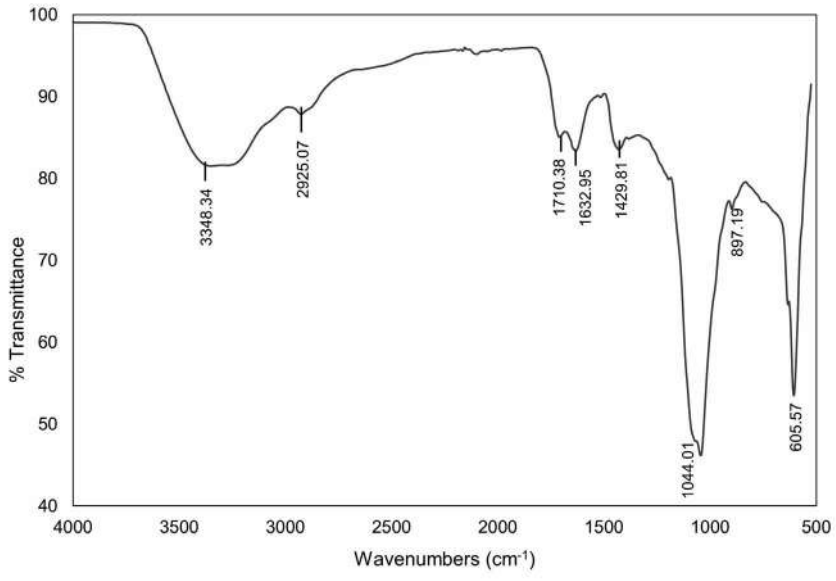

Fig. 1. FTIR spectrum of functional groups in lignin from durian rind

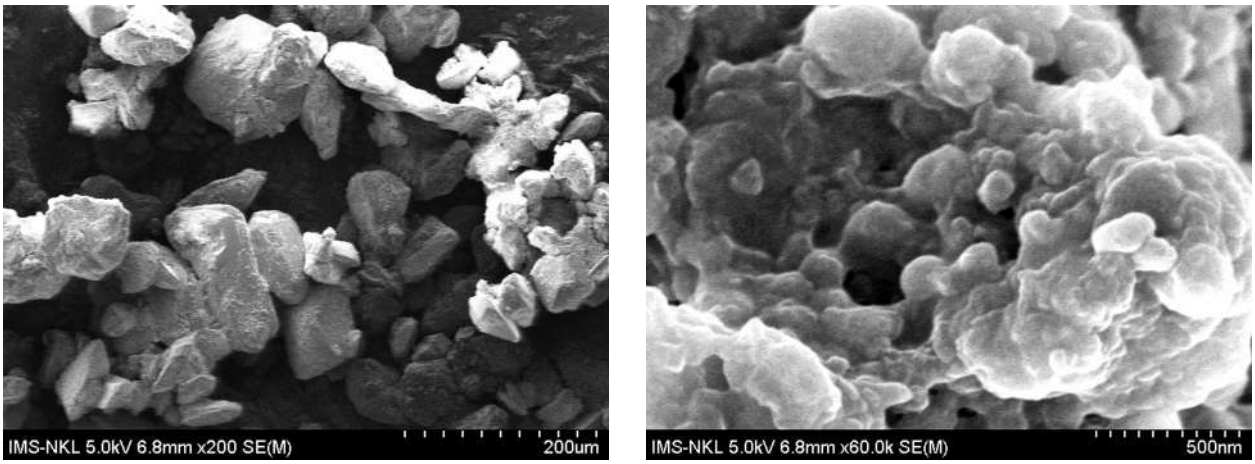

Fig. 3. SEM images of lignin from durian rind

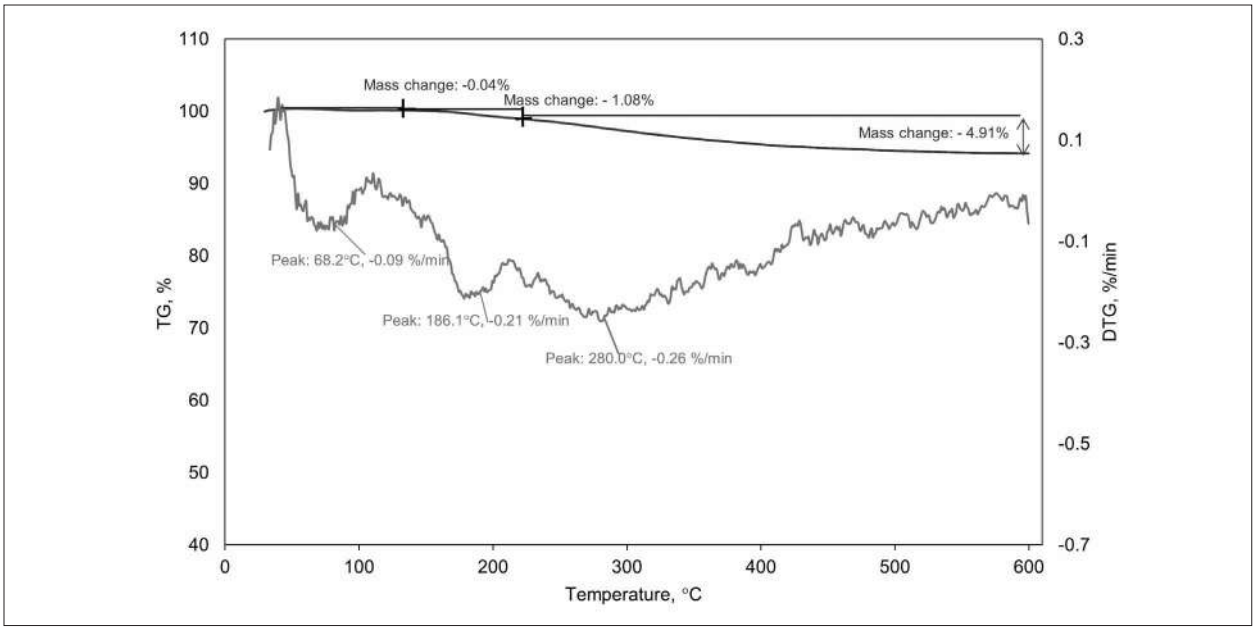

Fig. 4. TG and DTG plots of lignin from durian rind

adsorbent and the adsorbed substances, thereby facilitating their diffusion into the adsorbent material [50]. Similar structural features have been observed in lignin derived from rice husk [53, 54], Moroccan thuya [50], softwood kraft lignin nanoparticles [41], acetylated lignin [55], industrial lignin [56], lignin from sugarcane bagasse [30], and lignin extracted from native *Leucaena leucocephala* bark [51].

TG and DTG. Thermal analysis was conducted up to a temperature of 600 °C. The TGA curve in Figure 4 indicates that the thermal decomposition of lignin from DR is relatively low, with a maximum weight loss of approximately 5.84 % at 600 °C. This weight loss is distributed across three main regions: 30–100 °C, associated with the evaporation of moisture in the material [30, 57]; 180–220 °C, linked to the degradation of residual hemicellulose impurities [58]; and 240–360 °C, related to the decomposition of the lignin structure [30, 59]. The low weight loss of lignin suggests that it can be used under high temperature conditions without compromising the integrity of the adsorbent material.

Adsorption of MB by lignin from DR. Effect of pH. The ionization level of dye molecules and the surface charge of adsorbents were significantly impacted by the pH of the solution [30]. Therefore, pH played a crucial role in the adsorbent and adsorbate interaction. Thus, it was essential to investigate pH to determine the optimal conditions for the efficient performance of the adsorbent.

To evaluate the effect of pH in aqueous environments on adsorption capacity, experiments were conducted with pH values ranging

from 3 to 9, an initial MB concentration of 500 mg/L, an adsorbent dose of 10 g/L, and an adsorption time of 60 minutes. The results in Figure 5a showed that as the pH increased from 3 to 5, the adsorption of MB also rose. The highest adsorption capacity of MB by lignin occurred at pH 5. However, when the pH was further grew beyond 5, the efficiency of MB adsorption by lignin decreased.

In highly acidic conditions (pH 3), generating more H^+ ions led to competitive adsorption with MB^+ cations at lower pH levels [60]. As the pH level increased, the reduction in H^+ ions resulted in decreased competitive adsorption and increased adsorption efficiency [30]. Moreover, an increase in pH led to the deprotonation of carboxyl groups on the surface, increasing the negative charge and enhancing electrostatic attraction between MB molecules and lignin [61]. In an alkaline environment (pH≥7), the lignin surface was surrounded by OH^- groups, which made it more challenging for MB molecules to contact the lignin, thereby reducing adsorption efficiency and effectiveness [60]. Similar findings showed that the highest MB adsorption capacity using modified sugarcane bagasse occurred at pH 5 [30]. Therefore, lignin from DR demonstrated the best MB adsorption performance under mildly acidic conditions. For industrial wastewater treatment involving lignin under acidic or alkaline conditions, it is necessary to neutralize the water to a pH of 5 for the adsorbent to operate more effectively.

Effect of adsorbent dosage. The adsorbent dosage increased the adsorption capacity; however, using an excessive amount of adsorbent failed to enhance adsorption efficiency and resulted in wastage [31]. Therefore, it was essential to determine and select an appropriate adsorbent dosage. The study results on the effect of adsorbent dosage, conducted under conditions of pH 5, initial MB concentration of 500 mg/L, and an adsorption time of 60 minutes, shown in Figure 5b, indicated that when the adsorbent dosage was increased from 2 g/L to 10 g/L, both adsorption efficiency and MB removal efficiency

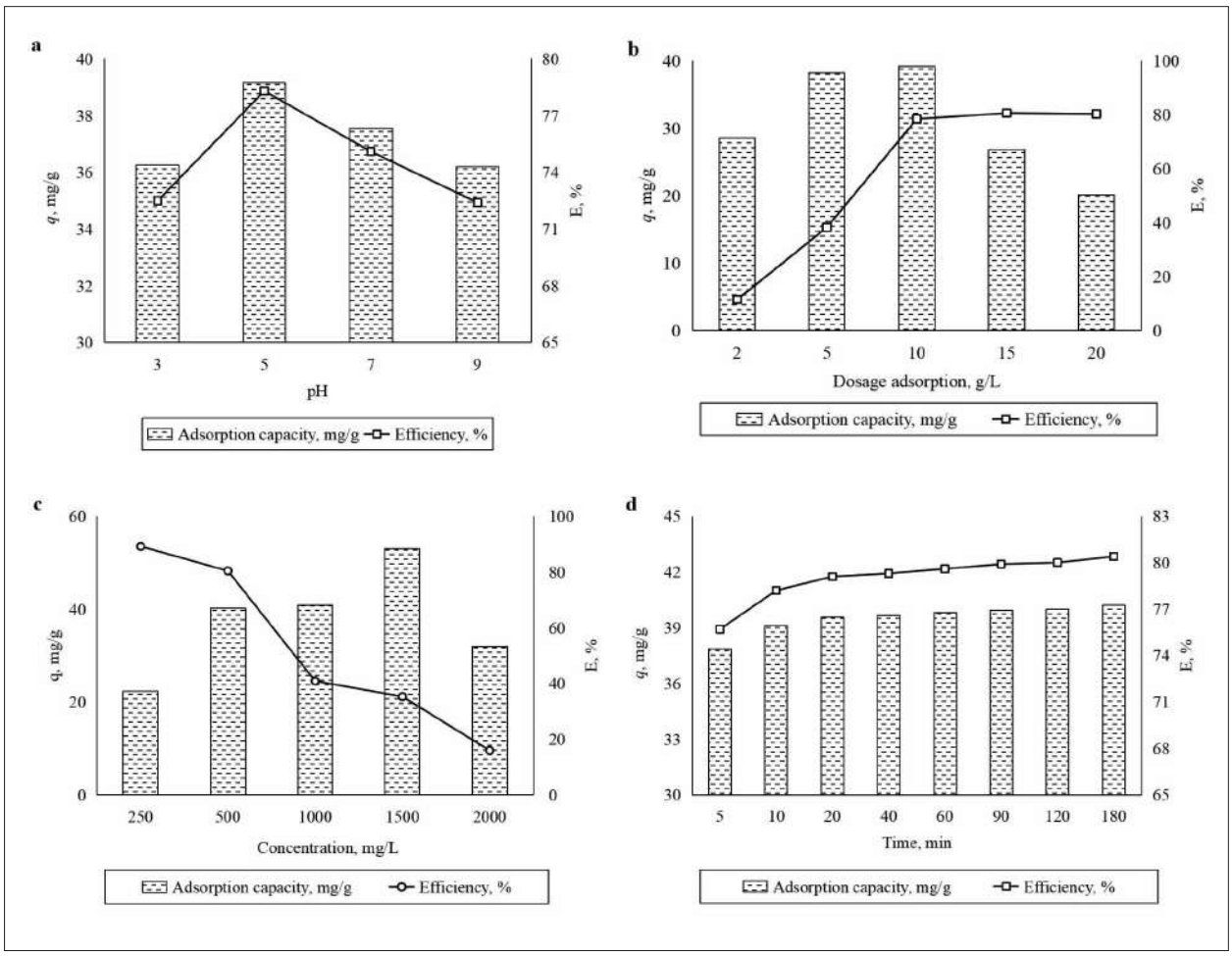

Fig. 5. Effect of pH (a), adsorbent dosage (b), time (c), and initial methylene blue (MB) concentration (d) on the efficiency of MB removal and MB adsorption capacity by lignin from durian rind

significantly improved. However, further increasing the lignin dosage to 15 g/L and 20 g/L decreased adsorption efficiency, and MB removal efficiency reached equilibrium. This could be attributed to the increased surface area for interaction between the adsorbate and the adsorbent, thereby enhancing adsorption efficiency [31, 62, 63]. Even with the adsorbent dosage exceeding 10 g/L, the incremental increase in pollutant removal efficiency became negligible and led to wastage, making the process economically inefficient. Therefore, the optimal adsorbent dosage was 10 g/L.

Effect of initial MB concentration. The initial concentration of the contaminant significantly affected the adsorption efficiency of the adsorbent. This study investigated initial MB concentrations ranging from 250 to 2000 mg/L under conditions of pH 5, an adsorption time of 60 minutes, and an adsorbent dose of 10 g/L. The results shown in Figure 5c indicated that increasing the initial MB concentration from 250 to 1500 mg/L significantly stimulated the adsorption efficiency. However, when the MB concentration exceeded 1500 mg/L, the adsorption efficiency decreased.

At low initial MB concentrations, MB^+ cations moved freely and were easily "captured" by lignin particles in the solution, resulting in higher adsorption efficiency than at higher initial MB concentrations [30, 60]. When the initial contaminant concentration was too high, a gradient layer formed around the adsorbent particles, hindering the penetration of the adsorbate into the pores or voids of the adsorbent. Thus, increasing the initial MB concentration from 1500 to 2000 mg/L decreased the adsorption efficiency [32, 64].

However, higher initial MB concentrations in the solution led to significantly reduced MB removal efficiency by lignin. When the MB concentration in the solution was below 500 mg/L, DR lignin could remove MB relatively efficiently, with removal efficiency reaching up to 89.2%. When the initial MB concentration was 1000 mg/L, the removal efficiency dropped below 40%. Therefore, dilution of the wastewater or multiple adsorption processes could be carried out for wastewater containing high concentrations of contaminants until the required contaminant concentration was achieved.

Effect of contact time. The influence of contact time on the adsorption efficiency and removal of MB dye in water was illustrated in Figure 5d. The MB adsorption process on DR lignin unfolded in three distinct stages: initially, the adsorption was notably rapid within the first 20 minutes. From minute 20 to 60, MB adsorption onto DR lignin particles decelerated as most adsorption sites on the adsorbent surface became occupied. Beyond 60 minutes, the adsorption reached equilibrium.

This phenomenon could be elucidated as follows: during the initial stage of the adsorption process, vacant adsorption sites on the adsorbent surface facilitated easy interaction and occupation by adsorbate molecules, resulting in rapid adsorption. As the process entered its second stage, the diminishing number of available adsorption sites made it progressively challenging for adsorbate molecules to find unoccupied sites, slowing the adsorption rate. By the third stage, nearly all accessible adsorption sites had been occupied, leading to an equilibrium where no substantial increase in efficiency was observed. Similar mechanisms have been reported in MB adsorption studies utilizing hybrid materials from technical lignins [32], activated carbon–clay composite [65], and polyurethane materials combined with chitin for oil adsorption [31].

Based on the data from Figure 5d, it was evident that the MB adsorption onto DR lignin reached equilibrium at 60 minutes, achieving an MB removal efficiency of 79.6%. The highest MB removal efficiency with DR lignin in water was 80.4 % after 180 minutes. Notably, within 20 minutes of adsorption, DR lignin effectively removed between 75.7% and 79.1% of the initial MB concentration. This performance was comparable to MB treatment efficiencies achieved using hybrid materials from technical lignins (80%) [64], surpassing those using ZnO nanoparticles (72%) [66] and periodiated modified nanocellulose (78%) [67].

Kinetic adsorption. The adsorption kinetics were studied to determine the rate, adsorption time, and mechanism of MB adsorption on lignin from DR [3, 30–32, 40]. pseudo-first-order, pseudo-second-order, intraparticle diffusion models and the Boyd equation were examined based on experimental data. The study established adsorption kinetics at pH 5, with an adsorbent dose of 10 g/L, an initial MB concentration of 500 mg/L, and contact times ranging from 5 to 180 minutes. The results and model fittings are shown in Figure 6 and Table 1.

From Figure 6a, it was observed that the plot of $\ln(q_e\text{-}q_t)$ against t was nonlinear, with a correlation coefficient R^2 of 0.8466, which was relatively low. Additionally, there was a significant difference between the experimental adsorption capacity ($q_{e,exp}$=40.2 mg/g) and the

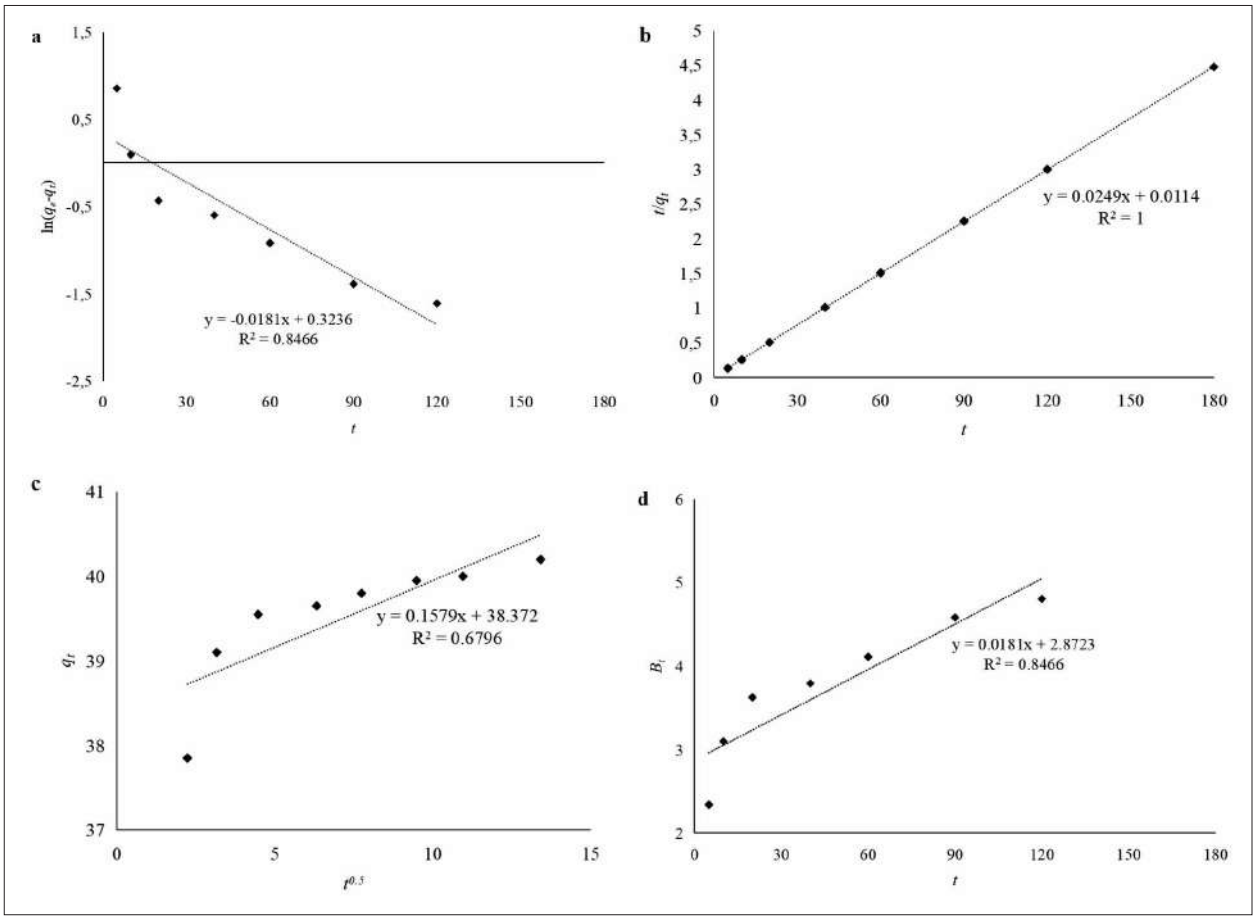

Fig. 6. Kinetic models of methylene blue adsorption by lignin from durian rind following the models: a – pseudo-first-order, b – pseudo-second-order, c – intraparticle diffusion, d – Boyd equation

Table 1

Kinetic parameters for the methylene blue adsorption by lignin from durian rind

Type of kinetic model	Parameters, unit	Value
Pseudo-first-order	$q_{e,\,exp}$, mg·g^{-1}	40.2
	$q_{e,cal}$, mg·g^{-1}	1.3821
	k_1, 1·min^{-1}	0.0181
	R^2	0.8466
Pseudo-second-order	$q_{e,\,exp}$, mg·g^{-1}	40.2
	$q_{e,\,cal}$, mg·g^{-1}	40.1606
	k_2, g.mg^{-1}·min^{-1}	0.0555
	h, mg·g^{-1}·min^{-1}	87.7193
	R^2	1.0
Intraparticle diffusion	k_p, mg·g^{-1}·min$^{-0.5}$	0.1579
	C	38.372
	R^2	0.6796
Boyd equation	R^2	0.8466

calculated capacity ($q_{e,cal}$=1.3821 mg/g) based on the model. This discrepancy indicated that the experimental results of MB adsorption on lignin did not fit well with the pseudo-first-order model.

The relationship between t/q_t and t in Figure 6b showed a linear correlation with a relatively high correlation coefficient (R^2=1), indicating that the Pseudo-second-order model best described the MB adsorption process on

DR lignin. Furthermore, the experimental adsorption capacity values ($q_{e,exp}$=40.2 mg/g) and the calculated values ($q_{e,cal}$=40.1606 mg/g) in Table 1 were nearly identical, confirming that the Pseudo-second-order model was suitable for predicting the maximum adsorption capacity of MB on DR lignin. Adhering to the Pseudo-second-order model implies that MB adsorption on DR lignin occurred through chemical interaction between MB and DR lignin [31, 39]. The initial adsorption rate value h for MB on DR lignin was 87.7193 mg/g·min, indicating that the adsorption rates of MB on DR lignin occurred relatively rapidly.

The intraparticle diffusion model was investigated to identify the diffusion type controlling the mass transfer rate based on the relationship between q_t and $t^{0.5}$. It was assumed that this relationship was nonlinear; two or more simultaneous adsorption mechanisms occurred, where boundary layer diffusion controlled the mass transfer rate [3, 32, 64, 68]. If the q_t versus $t^{0.5}$ plot was linear and passed through the origin, particle diffusion controlled the mass transfer rate [3, 31, 40, 64, 68]. In cases where the q_t versus $t^{0.5}$ plot was linear but did not pass through the origin, intraparticle diffusion occurred. Still, diffusion within the particle did not control the mass transfer rate [3, 64, 68]. Figure 6c demonstrated that the q_t versus $t^{0.5}$ plot was nonlinear and did not pass through the origin, confirming that diffusion controlled the mass transfer rate and that the MB adsorption process on DR lignin involved multiple adsorption mechanisms such as surface diffusion, pore diffusion, and surface interaction at active sites on the adsorbent [3, 32, 64, 68]. The higher the constant C was, the greater the influence of the boundary layer on the adsorption rate was observed [68]. The constant C obtained from Table 1 was 38.372, indicating that boundary layer diffusion influenced MB adsorption on DR lignin significantly [68].

The Boyd equation was studied to provide insights into the rate-limiting step of adsorption [3]. If the plot of B_t versus t was nonlinear or linear but did not pass through the origin, external film diffusion or boundary layer diffusion would be the rate-limiting step of adsorption; conversely, if the relationship B_t - t was linear and passed through the origin, pore diffusion would be the rate-limiting step of adsorption [3, 38, 69]. Figure 6d showed that the relationship between B_t and t was nonlinear (R^2=0.8466) and did not pass through the origin, implying that MB adsorption on DR lignin was limited by external film diffusion [3, 38, 69]. The results of the isotherm study using the Boyd equation were consistent with the analysis based on the intraparticle model.

Isotherm adsorption. The adsorption isotherm represents an equilibrium relationship describing how pollutants interact with an adsorbent material. Isothermal studies provide information about adsorption parameters, mechanisms, surface properties, and affinity between adsorbent and adsorbate [3, 4, 70]. The Langmuir, Freundlich, Dubinin-Radushkevich, and Temkin isotherm models are commonly used to characterize the interaction between adsorbents and adsorbates [3, 4]. Linear plots and parameters of the MB adsorption isotherm models on DR lignin were presented in Figure 7 and Table 2 under the conditions of pH 5, adsorbent dose of 10 g/L, adsorption time of 60 minutes, and initial MB concentration of 500 mg/L.

The experimental data in Figure 7 showed that the highest correlation coefficient R^2 was observed with the Langmuir model, R^2=0.9878. It confirmed that the experimental process of MB adsorption on DR lignin best fitted the mathematical description of the Langmuir model, characteristic of monolayer adsorption on a homogeneous surface without interaction between MB molecules [3, 32]. Additionally, the Langmuir model implied that the MB adsorption process on DR lignin occurred across the entire surface of the material with uniform adsorption energy [3, 71]. When MB molecules occupied the active sites on the adsorbent, other MB molecules could not occupy the same adsorption sites [3, 33]. The maximum adsorption capacity of MB on DR lignin was predicted to be 55.5556 mg/g. A higher value K_L of the Langmuir model indicated lower free energy of adsorption and stronger affinity between the adsorbate and adsorbent [3]. For the MB adsorption process on DR lignin, K_L was found to be 12.8571, indicating strong binding between MB and DR lignin during adsorption. The value R_L of $0 < R_L$=0.2839 < 1 indicated favourable dye adsorption on the material surface under study [17, 37, 70, 72].

For the Freundlich isotherm model, the correlation coefficient between the experimental data and the model was lower, R^2=0.8457, indicating that the Freundlich model was unsuitable for describing the MB adsorption process on DR lignin. The Freundlich constant (K_F), which relates to the adsorption capacity of the adsorbent material, was relatively low at 5.4915 mg/g, indicating a high demand for free energy in the MB adsorption process on DR lignin. The value of the Freundlich parameter $0 < 1/n$=0.1909

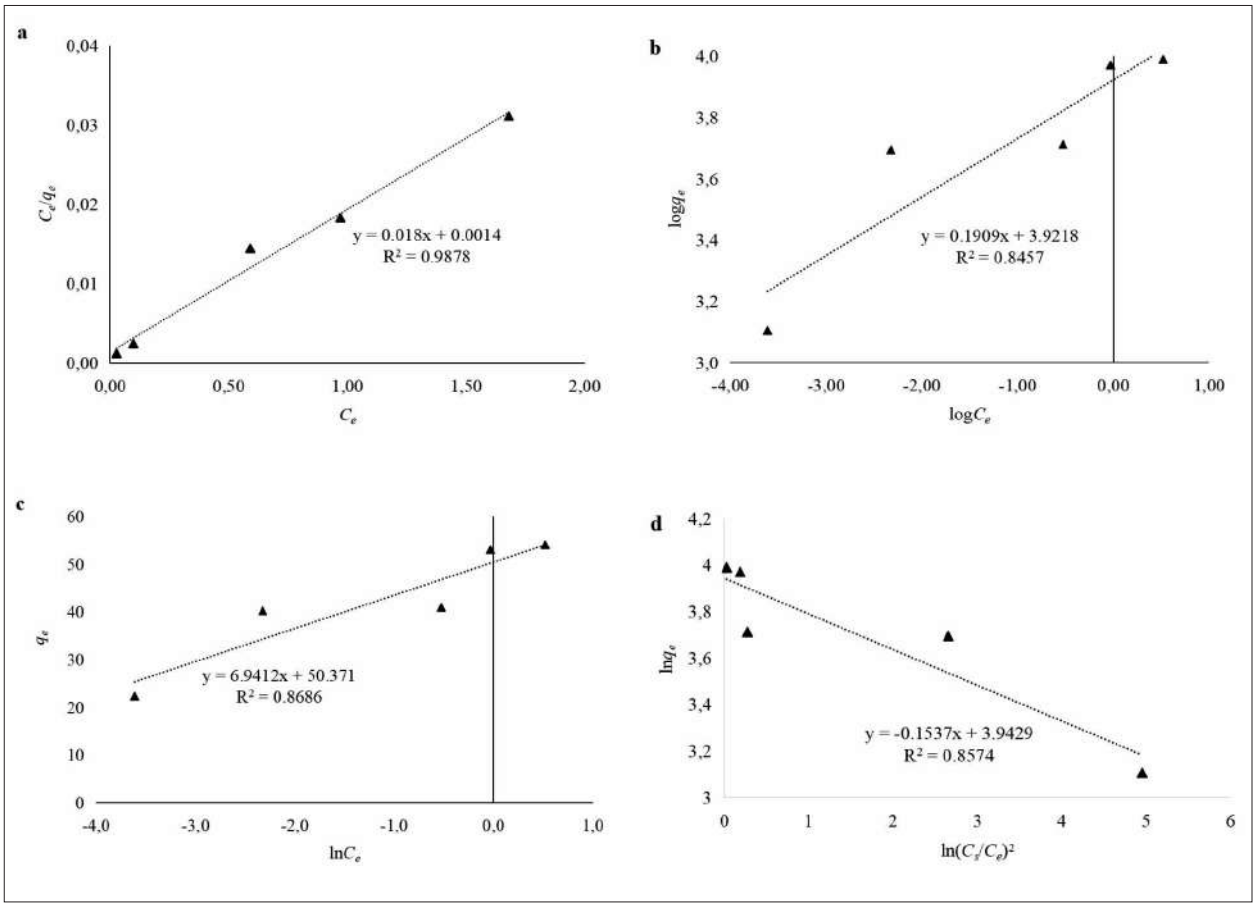

Fig. 7. Langmuir (a), Freundlich (b), Temkin (c) and Dubinin-Radushkevich (d) isotherm graphical plot for methylene blue removal by lignin from durian rind

Table 2

Parameters of adsorption isotherm models of methylene blue onto lignin from durian rind

Type of isotherm model	Parameters, unit	Value
Langmuir	q_m, mg·g^{-1}	55.5556
	K_L, L·mg^{-1}	12.8571
	R_L	0.2839
	R^2	0.9878
Freundlich	K_F, mg·g^{-1}	5.4915
	n	5.2383
	$1/n$	0.1909
	R^2	0.8457
Temkin	a_{TE}, L·g^{-1}	1.1477
	b_{TE}, kJ·mol^{-1}	0.3569
	R^2	0.8686
Dubinin-Radushkevich	E, kJ·mol^{-1}	4.0149
	q_m, mg·g^{-1}	0.3569
	R^2	0.8574

< 1 suggested favorable conditions for the MB adsorption process on DR lignin [17, 33]. The value of n=5.2383 > 1 indicated that the adsorption sites with the highest binding energies were utilized first on less heterogeneous surfaces, followed by weaker sites on more heterogeneous surfaces [3].

The energy parameter obtained from the D-R model indicated that the adsorption energy of MB on DR lignin was 4.0149 kJ/mol (<8 kJ/mol), suggesting that the MB adsorption process on DR lignin was predominantly physical adsorption [3, 37, 72]. It affirmed that the adsorption of MB on DR lignin primarily stemmed from electrostatic interactions and Van-der-Waals forces [37, 72].

Evaluation of the Temkin isotherm model provided information about the heat of adsorption of MB onto the adsorbent [72]. The value of the Temkin constant b_{TE} from the model was 0.3569 kJ/mol (>0), indicating that the adsorption of MB on DR lignin was an endothermic process and not spontaneous [17, 72, 73].

Based on the kinetic and adsorption isotherm studies, the interaction mechanism between MB and DR lignin is proposed. The primary mechanism for MB adsorption onto DR lignin involves electrostatic interactions between the positively charged nitrogen atoms in the MB molecule and the carboxyl and hydroxyl groups in the lignin molecule. Additionally, the interaction between MB and DR lignin may occur through hydrogen bonding and π-interactions.

Conclusion

This study aimed to recover lignin from agricultural waste durian rind to remove MB dye from water environments. The surface properties of DR lignin demonstrated its effective adsorption capability as a natural material. The conditions for MB adsorption by DR lignin were optimized at pH 5, an adsorbent dose of 10 g/L, and a contact time of 60 minutes. The maximum MB adsorption capacity of DR lignin reached 53 mg/g with a removal efficiency of up to 80.2%. The MB adsorption process on DR lignin followed pseudo-second-order kinetics and the Langmuir adsorption isotherm model, indicating monolayer adsorption on a homogeneous surface with chemical interactions between MB molecules and DR lignin. Investigation using the intraparticle diffusion model and Boyd equation suggested that MB adsorption on DR lignin was significantly influenced by boundary layer diffusion and primarily limited by film diffusion. The process involved multiple simultaneous adsorption mechanisms, including electrostatic interactions, hydrogen bonding, and π-π interactions during MB adsorption on DR lignin. Overall, lignin recovered from DR and agricultural waste generally shows promise as an economical adsorbent material for dye treatment in wastewater. This approach addresses the challenge posed by vast amounts of agricultural waste, produces economically valuable products, and provides potential adsorbents for industrial dye treatment in aqueous environments.

The authors would like to thank to HaUI Institute of Technology (HIT) and Hanoi University of Industry (HaUI, Hanoi, Vietnam) for providing the necessary laboratory support to gather data for this research article.

References

1. Oladoye P.O., Ajiboye T.O., Omotola E.O., Oyewola O.J. Methylene blue dye: Toxicity and potential elimination technology from wastewater // Results Eng. 2022. V. 16. Article No. 100678. doi: 10.1016/j.rineng.2022.100678

2. Eldeeb T.M., Aigbe U.O., Ukhurebor K.E., Onyancha R.B., El-Nemr M.A., Hassaan M.A., Ragab S., Osibote O.A., El Nemr A. Adsorption of methylene blue (MB) dye on ozone, purified and sonicated sawdust biochars // Biomass Conv. Bioref. 2024. V. 14. No. 8. P. 9361–9383. doi: 10.1007/s13399-022-03015-w

3. Trang T.Y.D., Zenitova L.A., Quynh P.H., Huong T.T., Dung L.H. Adsorption kinetic and isotherm of the oil spill onto adsorbents based on polyurethane foam grafted chitin and its modifications // Environment and Ecology Research. 2023. V. 11. No. 3. P. 513–526. doi: 10.13189/eer.2023.110311

4. Fito J., Abrham S., Angassa K. Adsorption of methylene blue from textile industrial wastewater onto activated carbon of *Parthenium hysterophorus* // Int. J. Environ. Res. 2020. V. 14. No. 5. P. 501–511. doi: 10.1007/s41742-020-00273-2

5. Hassaan M.A., El Nemr A. Pesticides pollution: Classifications, human health impact, extraction and treatment techniques // Egypt J. Aquat. Res. 2020. V. 46. No. 3. P. 207–220. doi: 10.1016/j.ejar.2020.08.007

6. Al-Ghouti M.A., Al-Absi R.S. Mechanistic understanding of the adsorption and thermodynamic aspects of cationic methylene blue dye onto cellulosic olive stones biomass from wastewater // Sci. Rep. 2020. V. 10. No. 1. Article No. 15928. doi: 10.1038/s41598-020-72996-3

7. Santoso E., Ediati R., Kusumawati Y., Bahruji H., Sulistiono D.O., Prasetyoko D. Review on recent advances of carbon based adsorbent for methylene blue removal from waste water // Mater. Today Chem. 2020. V. 16. Article No. 100233. doi: 10.1016/j.mtchem.2019.100233

8. Ye J.W., Nyobe D., Tang B., Bin L.Y., Li P., Huang S.S., Fu F.L., Cai Y.H., Guan G.Q., Hao X.G. Facilely synthesized recyclable mesoporous magnetic silica composite for highly efficient and fast adsorption of methylene blue from wastewater: Thermodynamic mechanism and kinetics study // J. Mol. Liq. 2020. V. 303. Article No. 112656. doi: 10.1016/j.molliq.2020.112656

9. Jawad A.H., Abdulhameed A.S., Reghioua A., Yaseen Z.M. Zwitterion composite chitosan-epichlorohydrin/zeolite for adsorption of methylene blue and reactive red 120 dyes // Int. J. Biol. Macromol. 2020. V. 163. P. 756–765. doi: 10.1016/j.ijbiomac.2020.07.014

10. Titchou F.E., Akbour R.A., Assabbane A., Hamdani M. Removal of cationic dye from aqueous solution using Moroccan pozzolana as adsorbent: Isotherms, kinetic studies, and application on real textile wastewater treatment // Groundwater Sustainable Dev. 2020. V. 11. Article No. 100405. doi: 10.1016/j.gsd.2020.100405

11. Temel F., Turkyilmaz M., Kucukcongar S. Removal of methylene blue from aqueous solutions by silica gel supported calyx[4]arene cage: Investigation of adsorption properties // Eur. Polym. J. 2020. V. 125. Article No. 109540. doi: 10.1016/j.eurpolymj.2020.109540

12. Vargas V.H., Paveglio R.R., Pauletto P. de S., Salau N.P.G., Dotto L.G. Sisal fiber as an alternative and cost-effective adsorbent for the removal of methylene blue and reactive black 5 dyes from aqueous solutions // Chem. Eng. Commun. 2020. V. 207. No. 4. P. 523–536. doi: 10.1080/00986445.2019.1605362

13. Khattab T.A., Abdelrahman M.S., Rehan M. Textile dyeing industry: environmental impacts and remediation // Environ. Sci. Pollut. Res. Int. 2020. V. 27. No. 4. P. 3803–3818. doi: 10.1007/s11356-019-07137-z

14. Lin Q., Wang K., Gao M., Bai Y., Chen L., Ma H. Effectively removal of cationic and anionic dyes by pH-sensitive amphoteric adsorbent derived from agricultural waste-wheat straw // J. Taiwan Inst. Chem. Eng. 2017. V. 76. P. 65–72. doi: 10.1016/j.jtice.2017.04.010

15. Tsade H., Anshebo S.T., Sabir F.K. Preparation and characterization of functionalized cellulose nanomaterials (CNMs) for Pb(II) ions removal from wastewater // J. Chem. 2021. V. 2021. No. 1. Article No. 5514853. doi: 10.1155/2021/5514853

16. Ama O.M., Wilson A.W., Ray S.S. Photoelectrochemical degradation of methylene blue dye under visible light irradiation using EG/Ag-ZrO_2 nanocomposite electrodes // Int. J. Electrochem. Sci. 2019. V. 14. No. 10. P. 9982–10001. doi: 10.20964/2019.10.41

17. Putro J.N., Santoso S.P., Soetaredjo F.E., Ismadji S., Ju Y.-H. Nanocrystalline cellulose from waste paper: Adsorbent for azo dyes removal // Environ. Nanotechnol. Monit. Manage. 2019. V. 12. Article No. 100260. doi: 10.1016/j.enmm.2019.100260

18. Tang Y., Lin T., Jiang C., Zhao Y., Ai S. Renewable adsorbents from carboxylate-modified agro-forestry residues for efficient removal of methylene blue dye // J. Phys. Chem. Solids. 2021. V. 149. Article No. 109811. doi: 10.1016/j.jpcs.2020.109811

19. Kang Z., Jia X., Zhang Y., Kang X., Ge M., Liu D., Wang C., He Z. A Review on application of biochar in the removal of pharmaceutical pollutants through adsorption and persulfate-based AOPs // Sustainability. 2022. V. 14. No. 16. Article No. 10128. doi: 10.3390/su141610128

20. Moges A., Nkambule T.T.I., Fito J. The application of GO-Fe_3O_4 nanocomposite for chromium adsorption from tannery industry wastewater // J. Environ. Manage. 2022. V. 305. Article No. 114369. doi: 10.1016/j.jenvman.2021.114369

21. Bedada D., Angassa K., Tiruneh A., Kloos H., Fito J. Chromium removal from tannery wastewater through activated carbon produced from *Parthenium hysterophorus* weed // Energy Ecol. Environ. 2020. V. 5. No. 3. P. 184–195. doi: 10.1007/s40974-020-00160-8

22. Tebeje A., Worku Z., Nkambule T.T.I., Fito J. Adsorption of chemical oxygen demand from textile industrial wastewater through locally prepared bentonite adsorbent // Int. J. Environ. Sci. Technol. 2022. V. 19. No. 3. P. 1893–1906. doi: 10.1007/s13762-021-03230-4

23. Trang T.Y.D., Pham H.Q., Huong T.T., Hanh D.T., Dzung H.T., Lan V.P. Application of response surface methodology for statistical optimization of the pectin recovery from durian peel // Food Sci. Technol. 2024. V. 12. No. 2. P. 128–146. doi: 10.13189/fst.2024.120202

24. Bhat R., Paliyath G. Fruits of tropical climates: Biodiversity and dietary importance // Encycl. Food Health. 2016. P. 138–143. doi: 10.1016/B978-0-12-384947-2.00337-8

25. Zhang S., Wang Z., Zhang Y., Pan H., Tao L. Adsorption of methylene blue on organosolv lignin from rice straw // Procedia Environ. Sci. 2016. V. 31. P. 3–11. doi: 10.1016/j.proenv.2016.02.001

26. Wang T., Jiang M., Yu X., Niu N., Chen L. Application of lignin adsorbent in wastewater treatment: A review // Sep. Purif. Technol. 2022. V. 302. Article No. 122116. doi: 10.1016/j.seppur.2022.122116

27. Zhang J., Lin X., Luo X., Zhang C., Zhu H. A modified lignin adsorbent for the removal of 2,4,6-trinitrotoluene // Chem. Eng. J. 2011. V. 168. No. 3. P. 1055–1063. doi: 10.1016/j.cej.2011.01.083

28. Saad R., Radovic-Hrapovic Z., Ahvazi B., Thiboutot S., Ampleman G., Hawari J. Sorption of 2,4-dinitroanisole (DNAN) on lignin // J. Environ. Sci. 2012. V. 24. No. 5. P. 808–813. doi: 10.1016/S1001-0742(11)60863-2

29. Zhang Z., Chen Y., Wang D., Yu D., Wu C. Lignin-based adsorbents for heavy metals // Ind. Crops Prod. 2023. V. 193. Article No. 116119. doi: 10.1016/j.indcrop.2022.116119

30. Nguyen-Thi N.Y., Nguyen C.Q., Le Dang Q., De Tran Q., Do-Thi T.N., Vu Thanh L.H. Extracting lignin from sugarcane bagasse for methylene blue and hexavalent chromium adsorption in textile wastewater: a facile, green, and sustainable approach // RSC Adv. 2024. V. 14. No. 7. P. 4533–4542. doi: 10.1039/D3RA08007B

31. Trang T.Y.D., Zenitova L.A. Study on the sorption capacity of the adsorbent based on polyurethane and chitin to remove oil spills // PNRPU Bulletin. Chemical Technology and Biotechnology. 2019. No. 2. P. 33–47 (in Russian). doi: 10.15593/2224-9400/2019.2.03

32. Budnyak T.M., Aminzadeh S., Pylypchuk I.V., Sternik D., Tertykh V.A., Lindström M.E., Sevastyanova O. Methylene blue dye sorption by hybrid materials from technical lignins // J. Environ. Chem. Eng. 2018. V. 6. No. 4. P. 4997–5007. doi: 10.1016/j.jece.2018.07.041

33. Huong T.T., Trang T.Y.D. Removal of lead ions from aqueous media using rice husk modified with manganese oxide // Environ. Ecol. Res. 2023. V. 11. No. 2. P. 340–361. doi: 10.13189/eer.2023.110209

34. Tonk S., Rápó E. Linear and nonlinear regression analysis for the adsorption of remazol dye by Romanian brewery waste by-product, *Saccharomyces cerevisiae* // Int. J. Mol. Sci. 2022. V. 23. No. 19. Article No. 11827. doi: 10.3390/ijms231911827

35. Lv N., Wang X., Peng S., Zhang H., Luo L. Study of the kinetics and equilibrium of the adsorption of oils onto hydrophobic jute fiber modified via the sol-gel method // Int. J. Environ. Res. Public Health. 2018. V. 15. No. 5. Article No. 969. doi: 10.3390/ijerph15050969

36. Gunatilake S.K. Methods of removing heavy metals from industrial wastewater // J. Multidiscip. Eng. Sci. Studies. 2015. V. 1. No. 1. P. 12–18.

37. Galimova R.Z, Shaikhiev I.G., Sverguzova S.V. Processing the results of the study of adsorption processes using Microsoft Excel software. Kazan: Kazanskiy natsionalnyy issledovatelskiy tekhnologicheskiy universitet; Belgorod: BGTU im. V.G. Shukhova, 2017. 60 p. (in Russian).

38. Khalifa R.E., Omer A.M., Tamer T.M., Ali A.A., Ammar Y.A., Mohy Eldin M.S. Efficient eco-friendly crude oil adsorptive chitosan derivatives: kinetics, equilibrium and thermodynamic studies // Desalin. Water Treat. 2019. V. 159. P. 269–281. doi: 10.5004/dwt.2019.24166

39. Hao X., Liu H., Zhang G., Zou H., Zhang Y., Zhou M., Gu Y. Magnetic field assisted adsorption of methyl blue onto organo-bentonite // Appl. Clay Sci. 2012. V. 55. P. 177–180. doi: 10.1016/j.clay.2011.11.019

40. Vinhal J.O., Nege K.K., Lage M.R., de M. Carneiro J.W., Lima C.F., Cassella R.J. Adsorption of the herbicides diquat and difenzoquat on polyurethane foam: Kinetic, equilibrium and computational studies // Ecotoxicol Environ. Saf. 2017. V. 145. P. 597–604. doi: 10.1016/j.ecoenv.2017.08.005

41. Pourbaba R., Abdulkhani A., Rashidi A., Ashori A. Lignin nanoparticles as a highly efficient adsorbent for the removal of methylene blue from aqueous media // Sci. Rep. 2024. V. 14. No. 1. Article No. 9039. doi: 10.1038/s41598-024-59612-4

42. Jahan M.S., Chowdhury D.A.N., Islam M.K., Moeiz S.M.I. Characterization of lignin isolated from some nonwood available in Bangladesh // Bioresour. Technol. 2007. V. 98. No. 2. P. 465–469. doi: 10.1016/j.biortech.2006.01.005

43. Xu F., Geng Z.C., Liu C.F., Ren J.L., Sun J.X., Sun R.C. Structural characterization of residual lignins isolated with cyanamide activated hydrogen peroxide from various organosolvs pretreated wheat straw // J. Appl. Polym. Sci. 2008. V. 109. No. 1. P. 555–564. doi: 10.1002/app.25156

44. Xiao L.P., Shi Z.J., Xu F., Sun R.C., Mohanty A.K. Structural characterization of lignins isolated from *Caragana sinica* using FT-IR and NMR spectroscopy // Guang Pu Xue Yu Guang Pu Fen Xi. 2011. V. 31. No. 9. P. 2369–2376.

45. Cai Y., Li G., Nie J., Lin Y., Nie F., Zhang J., Xu Y. Study of the structure and biosynthetic pathway of lignin in stone cells of pear // Sci. Hortic. 2010. V 125. No. 3. P. 374–379. doi: 10.1016/j.scienta.2010.04.029

46. Tejado A., Peña C., Labidi J., Echeverria J.M., Mondragon I. Physico-chemical characterization of lignins from different sources for use in phenol-formaldehyde resin synthesis // Bioresour. Technol. 2007. V. 98. No. 8. P. 1655–1663. doi: 10.1016/j.biortech.2006.05.042

47. Rashid T., Kait C.F., Murugesan T. A "Fourier Transformed Infrared" compound study of lignin recovered from a formic acid process // Procedia Eng. 2016. V. 148. P. 1312–1319. doi: 10.1016/j.proeng.2016.06.547

48. Zhang Q., Li H., Guo Z., Xu F. High purity and low molecular weight lignin nano-particles extracted from acid-assisted MIBK pretreatment // Polymers (Basel). 2020. V. 12. No. 2. Article No. 378. doi: 10.3390/polym12020378

49. Faix O. Classification of lignins from different botanical origins by FT-IR spectroscopy // Holzforschung. 1991. V. 45. No. S1. P. 21–28. doi: 10.1515/hfsg.1991.45.s1.21

50. Saber M., El Hamdaoui L., El Moussaouiti M., Tabyaoui M. Extraction and characterization of lignin from Moroccan Thuya. Its application as adsorbent of methylene blue from aqueous solution // Cellul. Chem. Technol. 2022. V. 56. No. 1-2. P. 69–81. doi: 10.35812/CelluloseChemTechnol.2022.56.06

51. Md Salim R., Asik J., Sarjadi M.S. Chemical functional groups of extractives, cellulose and lignin extracted from native *Leucaena leucocephala* bark // Wood Sci. Technol. 2021. V. 55. No. 2. P. 295–313. doi: 10.1007/s00226-020-01258-2

52. Xu Y., Li K., Zhang M. Lignin precipitation on the pulp fibers in the ethanol-based organosolv pulping // Colloids Surf., A. 2007. V. 301. No. 1–3. P. 255–263. doi: 10.1016/j.colsurfa.2006.12.078

53. Marcelo P. da R., Paulo H.B., Daniele G.M., Juliana B.M., Jessica S. da S., Ana M.M.D. Extraction of organosolv lignin from rice husk under reflux conditions // Biological and Chemical Research. 2017. V. 2017. P. 87–98.

54. Shweta K., Jha H. Rice husk extracted lignin-TEOS biocomposites: Effects of acetylation and silane surface treatments for application in nickel removal // Biotechnol. Rep. 2015. V. 7. P. 95–106. doi: 10.1016/j.btre.2015.05.003

55. Harahap M., Perangin-Angin Y.A., Purwandari V., Goei R., Tok A.L.Y., Gea S. Acetylated lignin from oil palm empty fruit bunches and its electrospun nanofibres with PVA: potential carbon fibre precursor // Heliyon. 2023. V. 9. No. 3. Article No. e14556. doi: 10.1016/j.heliyon.2023.e14556

56. Qian H., Wang J., Yan L. Synthesis of lignin-poly(N-methylaniline)-reduced graphene oxide hydrogel for organic dye and lead ions removal // J. Bioresour. Bioprod. 2020. V. 5. No. 3. P. 204–210. doi: 10.1016/j.jobab.2020.07.006

57. Poletto M. Assessment of the thermal behavior of lignins from softwood and hardwood species // Maderas Cienc. Tecnol. 2017. V. 19. No. 1. P. 63–74. doi: 10.4067/S0718-221X2017005000006

58. Yan Q., Zhang H., Ketelboeter T., Peng Y., Wan C., Cai Z. Tuning thermal and graphitization behaviors of lignin *via* complexation with transition metal ions for the synthesis of multilayer graphene-based materials // RSC Adv. 2024. V. 14. No. 11. P. 7592–7600. doi: 10.1039/D3RA05881F

59. Yan Q., Li J., Zhang X., Zhang J., Cai Z. Synthetic bio-graphene based nanomaterials through different iron catalysts // Nanomaterials. 2018. V. 8. No. 10. Article No. 840. doi: 10.3390/nano8100840

60. Cao L.N.H., Luong H.V.T., Dang H.G., Pham M.H., Ly T.H.T., Ha T.T. The use of synthetic material Fe_3O_4/lignin for the processing of methylene blue // Can Tho University J. Sci. 2022. V. 58. No. 1. P. 1–16 (in Vietnamese). doi: 10.22144/ctu.jvn.2022.001

61. Utomo H.D., Phoon R.Y.N., Shen Z., Ng L.H., Lim Z.B. Removal of methylene blue using chemically modified sugarcane bagasse // Nat. Resour. 2015. V. 6. No. 4. P. 209–220. doi: 10.4236/nr.2015.64019

62. Saputra E., Saputra R., Nugraha M.W., Irianty R.S., Utama P.S. Removal of methylene blue from aqueous solution using spent bleaching earth // IOP Conf. Ser.: Mater. Sci. Eng. 2018. V. 345. Article No. 012008. doi: 10.1088/1757-899X/345/1/012008

63. Jin Y., Zeng C., L Q.-F., Yu Y. Efficient adsorption of methylene blue and lead ions in aqueous solutions by 5-sulfosalicylic acid modified lignin // Int. J. Biol. Macromol. 2019. V. 123. P. 50–58. doi: 10.1016/j.ijbiomac.2018.10.213

64. Piperopoulos E., Calabrese L., Mastronardo E., Abdul Rahim S.H., Proverbio E., Milone C. Assessment of sorption kinetics of carbon nanotube based composite foams for oil recovery application // J. Appl. Polym. Sci. 2019. V. 136. No. 14. Article No. 47374. doi: 10.1002/app.47374

65. Marrakchi F., Bouaziz M., Hameed B.H. Activated carbon–clay composite as an effective adsorbent from the spent bleaching sorbent of olive pomace oil: Process optimization and adsorption of acid blue 29 and methylene blue // Chem. Eng. Res. Des. 2017. V. 128. P. 221–230. doi: 10.1016/j.cherd.2017.10.015

66. Kahsay M.H. Synthesis and characterization of ZnO nanoparticles using aqueous extract of *Becium grandiflorum* for antimicrobial activity and adsorption of methylene blue // Appl. Water Sci. 2021. V. 11. No. 2. Article No. 45. doi: 10.1007/s13201-021-01373-w

67. Tsade Kara H., Anshebo S.T., Sabir F.K., Adam Workineh G. Removal of methylene blue dye from wastewater using periodiated modified nanocellulose // Int. J. Chem. Eng. 2021. V. 2021. Article No. 9965452. doi: 10.1155/2021/9965452

68. Sutherland C., Venkobachar C. A diffusion-chemisorption kinetic model for simulating biosorption using forest macro-fungus, *Fomes fasciatus* // Int. Res. J. Plant Sci. 2010. V. 1. No. 4. P. 107–117. doi: 10.6084/m9.figshare.6197030.v1

69. Hu Q., Liu Y., Feng C., Zhang Z., Lei Z., Shimizu K. Predicting equilibrium time by adsorption kinetic equations and modifying Langmuir isotherm by fractal-like approach // J. Mol. Liq. 2018. V. 268. P. 728–733. doi: 10.1016/j.molliq.2018.07.113

70. Nwadiogbu J.O., Ajiwe V.I.E., Okoye P.A.C. Removal of crude oil from aqueous medium by sorption on hydrophobic corncobs: Equilibrium and kinetic studies // J. Taibah Univ. Sci. 2016. V. 10. No. 1. P. 56–63. doi: 10.1016/j.jtusci.2015.03.014

71. Trang T.Y.D., Zenitova L.A. Polymer composite material based on polyurethane and chitin – the sorbent of heavy metal ions // Herald of Technological University. 2021. V. 24. No. 1. P. 26–31.

72. Hilma Siregar S., Wijaya K., Sri Kunarti E., Syoufian A., Suyanta. Kinetics adsorption of heavy oil spills in rivers on magnetite-(CTAB-montmorillonite) adsorbent // IOP Conf. Ser.: Mater. Sci. Eng. 2019. V. 509. Article No. 012136. doi: 10.1088/1757-899X/509/1/012136

73. Moughaoui F., Ouaket A., Eddebbagh M., Bennamara A., Abourriche A., Anbaoui Z., Berrada M. Study of adsorption isotherms and kinetic models of methylene blue adsorption on moroccan bagasse waste // ICABES-2017: proceedings of the 7th Int. Conf. on Innovation in Chemical, Agricultural, Biological and Environmental Sciences. London, 2017. P. 59–65. doi: 10.15242/HEAIG.H1217238